Trail formation based on directed pheromone deposition

Emmanuel Boissard[1,2] Pierre Degond[1,2]

Sebastien Motsch[3]

December 17, 2011

1-Université de Toulouse; UPS, INSA, UT1, UTM ;
Institut de Mathématiques de Toulouse ;
F-31062 Toulouse, France.
2-CNRS; Institut de Mathématiques de Toulouse UMR 5219 ;
F-31062 Toulouse, France.
email: emmanuel.boissard@math.univ-toulouse.fr ;
pierre.degond@math.univ-toulouse.fr

3-Department of Mathematics
University of Maryland
College Park, MD 20742-4015
email: smotsch@cscamm.umd.edu

Abstract

We propose an Individual-Based Model of ant-trail formation. The ants are modeled as self-propelled particles which deposit directed pheromone particles and interact with them through alignment interaction. The directed pheromone particles intend to model pieces of trails, while the alignment interaction translates the tendency for an ant to follow a trail when it meets it. Thanks to adequate quantitative descriptors of the trail patterns, the existence of a phase transition as the ant-pheromone interaction frequency is increased can be evidenced. We propose both kinetic and fluid descriptions of this model and analyze the capabilities of the fluid model to develop trail patterns. We observe that the development of patterns by fluid models require extra trail amplification mechanisms that are not needed at the Individual-Based Model level.

Acknowledgements: The authors wish to thank J. Gautrais, C. Jost and G. Theraulaz for fruitful discussions. P. Degond wishes to acknowledge the hospitality of the Mathematics Department of Tsinghua University where this research was completed. The work of S. Motsch is partially supported by NSF grants DMS07-07949, DMS10-08397 and FRG07-57227.

Key words: Self-propelled particles, pheromone deposition, directed pheromones, alignment interaction, Individual-Based Model, trail detection, pattern formation, kinetic models, fluid models

AMS Subject classification: 35Q80, 35L60, 82C22, 82C31, 82C70, 82C80, 92D50.

1 Introduction

One of the many features displayed by self-organized collective motion of animals or individuals is the formation of trails. For instance, ant displacements are characterized by their organization into lanes consisting of a large number of individuals, for the purpose of exploring the environment or exploiting its resources. Another example involving species with higher cognitive capacities is the formation of mountain trails by hikers or herds of animals. In both cases, the main feature is that the interaction between the individuals is not direct, but instead, is mediated by a chemical substance or by the environment. Indeed, ants lay down pheromones as chemical markers. These pheromones are sensed by other individuals which use them to adjust their path. In the case of mountain trails, the modification of the soil by walkers facilitates the passage of the next group of individuals and attracts them. This phenomenon is well-known to biologists under the name of stigmergy, a concept first forged by Pierre-Paul Grassé [23] to describe the coordination of social insects in nest building.

The formation of trails by ants has been widely studied in the biological literature [2, 14, 16–18, 48]. One general observation is the fact that trail formation is a self-organized phenomenon and expresses the emergence of a large-scale order stemming from simple rules at the individual level. Indeed, ant colonies in the numbers of thousands of individuals or more arrange into lines without resorting to long-range signaling or hierarchical organization. Another striking feature is the variability of the trail patterns, which may range from densely woven networks to a few large trails. This flexibility may result from the ability of the individuals to adapt their activity to variable external conditions such as food availability, temperature, terrain conditions, the presence of predators, etc. Trail plasticity derives from internal and external factors: for example it may vary according to the species of ant under consideration or depends on the properties of the soil. Our goal is to

provide a model that accounts for these two general facts: spontaneous formation of trails, and variability of the trail pattern.

At the mathematical level, several types of ant displacement and pheromone deposition models have been introduced. A first series of works deals with ant displacement on a pre-existing pheromone trail and focuses on the role of the antennas in the trail sensing mechanism [8, 9, 14]. Spatially one-dimensional models do not specifically address the question of trail build-up either, since motion occurs on a one-dimensional predefined trail. One-dimensional cellular automata models have been used to determine the fundamental diagram of pheromone-regulated traffic and to study the spontaneous break-up of bi-directional traffic in one preferred direction [30, 35].

The decision-making mechanisms which lead to the selection of a particular branch when several routes are available have been modeled by considering Ordinary Differential Equations (ODE's) for the global ant and pheromone densities on each trail [3,15,22,39]. These models do not account for the spontaneous formation of the trails. In [17], the spatial distribution of trails is ignored in a similar way. However, it introduces the concept of a space-averaged statistical distribution of trails, which reveals itself to be very effective. This model has been extended to include a one-dimensional spatial dependence in [47]. In the present work, we have borrowed from [17, 47] the idea of considering trails as particles in the same fashion as ants, and of dealing with them through the definition of a trail distribution function. However, by contrast to these works, we consider a two-dimensional model and keep track of both the spatial and directional distribution of the trails.

In general, two dimensional models assume that ant motion occurs on a fixed lattice. Two classes of ant models have been considered: Cellular Automata models [18,20,48], and Monte-Carlo models [3,15,40,41,44]. In the first class of models, no site can be occupied by more than one ant, while in the second class, ants are modeled as particles subject to a biased random walk on the lattice. In [46], the authors introduce some mean-field approximation of the previous models: a time-continuous Master equation formalism is used to determine the evolution of the ant density on each edge. In all these models, the jump probabilities are modified by the presence of pheromones. The presence of pheromones is modeled by a second species of particles which are deposited by the ants with a certain probability per unit time. Each particle corresponds to the amount of pheromone molecules contained in the deposited droplets (supposed constant in time and uniform among the ants). These pheromone particles can be located at the nodes of the lattice [40, 41, 44]. However, the trail reinforcement mechanism seems more efficient if these particles are located along the edges of the lattice [3, 15, 18, 20, 48]. To enhance the trail formation mechanisms, some authors [41,44] introduce two different chemical substances: an exploration pheromone which is deposited during foraging and a recruitment

pheromone which is laid down by ants who have found food and try to recruit congeners to exploit it. In [40], it is demonstrated that trail formation is enhanced by introducing some saturation of the ant sensitivity to pheromones at high pheromone concentrations. Inspired by the observation that pheromone deposition along the edges of the lattice seems to be more efficient in producing self-organized trails, we suppose that the laid down chemical substance gives rise to trails (i.e. the deposited quantities are vectors) rather than spots of substance concentration (usually modeled as scalar quantities).

All these previously cited two-dimensional models assume a pre-existing lattice structure. One question which is seldom addressed is whether this pre-existing lattice may influence the formation of the trails. For instance, it is well-known that lattice Boltzmann models with too few velocities have incorrect behavior. One may wonder if similar effects could be encountered with spatially discrete ant trail formation models. For this reason, in the present work, we will depart from a lattice-like spatial organization and treat the motion of the ants in the two-dimensional continuous space.

In this work, we propose a time and space continuous Individual-Based Model for self-organized trail formation. In this model, self-propelled particles interact by laying down pheromone trails that indicate both the position and direction of the trails. Ants adapt their course by following trails deposited by others, therefore reinforcing existing trails while pheromone evaporation allows weaker trails to disappear. The ant dynamics is time-discrete and is a succession of free flights and velocity jumps occuring at time intervals Δt. Velocity jumps occur with an exponential probability. Two kinds of velocity jumps are considered: purely random jumps which translate the ability of ants to explore a new environment, and trail-recruitment jumps. In order to perform the latter, ants look for trails in a disk around themselves, pick up one of these trails with uniform probability and adopt the direction of the chosen trail.

This model bears analogies with chemotaxis models. Chemotaxis is the name given to remote attraction interaction through chemical signaling in colonies of bacteria. Mathematical modeling of chemotaxis has been widely studied. Macroscopic models were first introduced by Keller and Segel in the form of a set of parabolic equations [32]. These equations can be obtained as macroscopic limits of kinetic models [19, 21, 27, 36, 37]. Kinetic models describe the evolution of the population density in position-velocity space. In [42] a direct derivation of the Keller-Segel model from a stochastic many-particle model is given. The common feature of most chemotaxis models is the appearance of blow-up, which corresponds to the fast aggregation of individuals at a specific point in space (see e.g. [5, 10]). By contrast, in the present paper, the dynamics gives rise to the spontaneous organization of lane-like spatial patterns, much alike to the observed behavior of ants. The rea-

son for this different morphogenetic behavior is the directed nature of the mediator of the interaction.

The model also bears analogies with the kinetic model of cell migration developed in [38]. In this model, cells move in a medium consisting of interwoven extra-cellular fibers in the direction of one, randomly chosen fiber direction. As they move, cells specifically destroy the extracellular fibers which are transverse to their motion. The induced trail reinforcement mechanism produces a network. There are two differences with the trail formation mechanism that we present here. The first one is that in [38] the dynamics start from a prescribed set of motion directions and gradually reduces this set, while our algorithms builds up the set of available directions gradually and new directions are created through random velocity jumps. The second difference is the role of trail evaporation in our algorithm, which has no equivalent in the cell motion model. Indeed, trail evaporation is a major ingredient for network plasticity.

In the last part of the present work, we derive a kinetic formulation of the proposed ant trail formation model in the spirit of [38]. Then, the fluid limit of this kinetic model is considered. We show that the resulting fluid model can exhibit trail formation only if some amplification mechanism is incorporated. Here, we consider that the ants choose the stronger trails with a higher probability than the weaker ones. By contrast, the Individual-Based Model produces trails even in the absence of such a mechanism. The Individual-Based Model possesses some stochasticity that may help the emergence of trails, a feature that the macroscopic model has lost.

The propensity to align with neighbors has been recognized as one of the major components of animal behavior, since the seminal work of Aoki [1]. This behavior is ubiquitous throughout a large range of scales, from insects [24] to birds [33] and has triggered a large physics literature, since the seminal work of Vicsek and coworkers [45]. It has been recently argued that the trend to align with others may be a consequence of other behavioral rules such as attraction and repulsion [31]. In the present work, we point out the importance of *mediated* alignment interaction through directed pheromone deposition. Pheromone deposition introduces a time delay: indeed, by this process, an ant can interact with the past positions and orientations of another ant. We show that, independently of the way this interaction builds up, the concept of a directed pheromone mediated alignment interaction can be a powerful paradigm to understand the emergence and morphologic diversity of ant trails. It could also possibly be applied to other biological morphogenesis phenomena (another example, pertaining to collective cell migration, has been mentioned above, and can be found in [38]).

The outline of this paper is as follows. In section 2, we provide the model description. Section 3 is devoted to the analysis of the simulations of the Individual-

Based Model. We establish a methodology for the detection of trail patterns from a simulation outcome, and analyze the dependency of the observed features on the model parameters. In section 4, we formally establish a set of kinetic equations that describes the dynamics and we investigate their fluid limit. A conclusion in section 5 draws some perspectives from this work.

2 An Individual-Based-Model of ant behavior based on directed pheromone deposition

2.1 Description of the model

We consider N "ants" in a flat (2-dimensional) domain: each ant is described by its position $x_i \in \mathbb{R}^2$ and the direction of its motion ω_i. The vector ω_i is supposed to be of unit-length, i.e. $\omega_i \in \mathbb{S}^1$, where $\mathbb{S}^1$ denotes the unit circle. We also consider pieces of trails described by pairs (x_p, ω_p) where $x_p \in \mathbb{R}^2$ is the trail piece position and ω_p is a unit vector describing the trail direction (see figure 1). In the case of ants, the marking of the trail is realized by a chemical marker, namely a trail pheromone. We assume that the ants can distinguishably perceive the direction of the trail of this chemical marker and that they are able to follow, not the line of steepest gradient, like in chemotaxis, but the direction of this trail. We provide arguments to support this assumption in section 2.2. Note that in the case of walkers or sheep in an outdoor terrain, the marking of the trail is realized by the modification of the terrain consecutive to the passage of the walkers, such as flattened grass. For polar bears, this modification is realized by the trail left in the snow by the animals. In the following, we concentrate on the modeling of ant trail formation, and we will indistinguishably refer to these pieces of trails as 'trails' or 'pheromone trails', or simply, 'pheromone particles'. The set of pheromone particles varies with time, since new pheromone particles are created by the deposition process and pheromone particles disappear after some time in order to model the evaporation process. We will denote by $\mathcal{P}(t)$ the set of pheromone particles at time t.

The simulated ants follow a random walk process. During its free motion phase, Ant i moves in direction ω_i at a constant speed c, i.e. is subject to the differential equation:

$$\dot{x}_i = c\omega_i, \quad \dot{\omega}_i = 0, \tag{2.1}$$

where the dots stand for time derivatives. This free motion is randomly interrupted by velocity jumps. When Ant i undergoes a velocity jump at time t, its velocity direction before the jump $\omega_i(t)^-$ is suddenly changed into a different one $\omega_i(t)^+$. The jump times are drawn according to Poisson distributions. In practice, a time discrete algorithm is used, with time steps Δt. With such a discretization, a Poisson

process of frequency λ is represented by an event occuring with probability $1-e^{-\lambda\Delta t}$ over this time step. There are two kinds of jumps: random velocity jumps and trail recruitment jumps.

Random velocity jumps. In this case, $\omega_i(t)^+$ differs from $\omega_i(t)^-$ by a random angle ε, i.e. $\widehat{(\omega_i(t)^-, \omega_i(t)^+)} = \varepsilon$, where ε is drawn out of a Gaussian distribution $p(\varepsilon)$ with zero mean and variance σ^2, periodized over $[0, 2\pi]$, i.e.

$$p(\varepsilon)\, d\varepsilon = \sum_{n\in\mathbb{Z}} \frac{1}{(2\pi\sigma^2)^{1/2}} \exp\left(-\frac{(\varepsilon+2n\pi)^2}{2\sigma^2}\right) d\varepsilon, \quad \varepsilon \in [0, 2\pi].$$

The frequency of the Poisson process is constant in time and denoted by λ_r.

Trail recruitment jump. In this case, $\omega_i(t)^+$, is chosen with uniform probability among the directions ω_p of the pheromone trails located in the ball $B_R(x_i(t))$ of radius R centered at $x_i(t)$ (see figure 1). $B_R(x_i(t))$ is the ant detection region and R its detection radius. More precisely, defining the set

$$S_i(t) = \{p \in \mathcal{P}(t)\,,\, |x_p - x_i(t)| \leq R\},$$

Ant i chooses an index p in $S_i(t)$ with uniform probability and sets

$$\omega_i(t)^+ = \omega_p. \tag{2.2}$$

This mechanism will be referred to as 'polar' interaction, because the ant adopts both the direction and orientation of the pheromone trail. A variant of this mechanism involves a non-polar interaction (i.e. the deposited trails have no specific orientation). This type of interaction is sometimes called 'nematic' [13] by reference to the liquid crystal terminology, but we will use the term 'non-polar' in this manuscript. In this case, the new direction is defined by

$$\omega_i(t)^+ = \pm\omega_p, \quad \text{such that} \quad \widehat{(\omega_i(t)^+, \omega_p)} \quad \text{is acute.} \tag{2.3}$$

The non-polar interaction makes more biological sense, since it seems difficult to envision a mechanism which would allow the ants to detect the orientation of a given trail. The use of a uniform probability to select the interacting pheromone particle can be questioned. For instance, the choice of the pheromone trail p could be dependent on the angle $\widehat{(\omega_i(t)^-, \omega_p)}$ as considered in [46], but in the present work we will ignore this effect. Ants may also preferably choose the largest trails indicated by a large concentration of pheromone substance in one given direction. This 'preferential choice' will be discussed in connection to the kinetic and fluid models in section 4 but discarded in the numerical simulations of the Individual-Based Model.

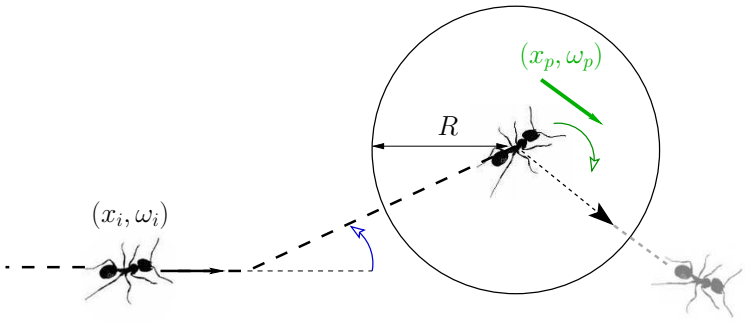


Figure 1: Ants follow a random walk process. Each ant is moving on a straight line until it undergoes a random velocity jump (left) or a trail recruitment jump (right). In this picture, a pheromone particle is located in the disk centered at the ant location when the jump occurs, and of given radius R.

The frequency of the Poisson process is given by $\lambda_p M_i(t)$ where $M_i(t)$ is the number of pheromone particles in the detection region of Ant i: $M_i(t) = |S_i(t)|$, and λ_p is the trail recruitment frequency per pheromone particle. The dependency of the jump frequency upon the number of detected pheromone particles accounts for the observed increase of the alignment probability with the pheromone density. Of course, nonlinear functions of the pheromone density could be chosen as well. For instance, some saturation of the detection capability occurs at large pheromone densities, such as investigated in [40]. This effect will also be ignored here. We also discard any consideration of the detection mechanism, such as discussed e.g. in [8, 9, 14].

During their walk, ants leave pheromone particles at a certain deposition rate ν_d. If at time t, ant i deposits a pheromone droplet, a new pheromone particle is created at position $x_i(t)$ with the direction $\omega_i(t)$. Hence, we postulate that:

At deposition times t, a pheromone particle p is created with :

$$(x_p, \omega_p) = (x_i(t), \omega_i(t)).$$

Pheromone particles have a life-time T_p and remain immobile during their lifetime. In this work, pheromone diffusion is neglected. Pheromone deposition and evaporation times are modeled by Poisson processes: each ant has a probability ν_d per unit of time to lay down a pheromone particle and each pheromone particle has a probability $1/T_p$ per unit of time to disappear.

Pheromone deposition mediates the interactions between the ants. This interaction is nonlocal in both space and time (because the ant which has deposited a pheromone particle may have moved away quite far before another ant interacts with it). Random velocity jumps and trail recruitment jumps have opposite effects.

Random velocity jumps generate diffusion at large scales whereas trail recruitment jumps tend to produce concentrations of the ants trajectories on the pheromone trails. Therefore, the pheromone-mediated interaction induces correlations of the ants motions and these correlations result in trail formation.

The trail recruitment process together with pheromone evaporation result in network plasticity. To illustrate this mechanism, let us consider the following simplified situation. Suppose an ant reaches a "crossroads" of trails, meaning a spot where two pheromone trails point in two different directions denoted by 1 and 2. Suppose there are n_1 pheromone particles pointing in one direction and n_2 in the other one. The probability for the ant to choose to orient in direction i; $i = 1, 2$, is equal to the ratio $\frac{n_i}{n_1+n_2}$. When the ant turns to its new direction, it may release a pheromone particle which will serve to reinforce this branch. Eventually, one underselected branch of the crossroads will vanish due to evaporation of the pheromones. Note that the choice of the surviving branch depends on random fluctuations of this process: therefore, the outcome of this situation is non-deterministic and even an initially strongly populated branch has a non-zero probability of vanishing away.

2.2 Biological relevance of the model assumptions

Ants produce pheromones through various glands such as the Dufour gland, the venom gland or the anal sac [34]. The pheromone is applied to the ground through the sting. Ants depositing pheromones bend their abdomen downward and extrude their sting. The tip of the sting touches the ground and deposits the pheromone in the very same way as a pen deposits ink [49]. Pheromone deposition can be observed by various means. The bending of the abdomen can be observed, either directly [49] or using video recording [2, 29]. Another technique uses a soot-coated glass panel [26, 28, 50]. When touching the glass, the ant sting and hair remove the soot and leave marks that can be recorded.

Using these techniques, various pheromone marking scenarios have been observed, corresponding to either different species or within the same species to different situations: continuous streaks [28], series of long broken streaks [28, 49], spotted trails with close spots (separated by the order of 0.03 mm) [28] (especially Fig. 2), spots separated by a couple of millimeters [26], spots separated by a distance of the order of a centimeter [29] or more [2]. Therefore, a large range of possibilities occur.

Continuous pheromone deposition by ants has been modeled in [7]. The combination of continuous deposition and evaporation leads to an analytical expression for the pheromone concentration known as Sutton's formula [43]. The two-dimensional concentration profile looks like a mountain ridge with a crest following the path of deposition. In the case of a continuous trail, the mechanism by which an ant orients itself along the trail, called osmotropotaxis, has been described and mod-

eled in [8, 9, 14]. By sensing the difference of pheromone concentrations at the tips of its two antennae, the ant is able to orient itself in the direction of the highest concentration. It results in an undulatory motion which in average follows the crest of the ridge formed by the pheromone concentration and leads to a trail following behavior. In this case, it is legitimate to say that ants deposit an oriented information, the pheromone trail and that the result of the osmotropotaxis mechanism is the choice of this direction of motion by the recruited ant. In this circumstance, our model is justified.

The case of discontinuous pheromone deposition has been modeled in [25]. In this case, diffusion contributes to wipe out the discontinuities of the deposition process. It leads to a pheromone concentration which takes the form of an irregular ridge with mounds at the location of the depositions points which are separated by mountain passes. If the diffusion coefficient D is large enough compared to the mean distance d separating successive deposition points, the concentration profile seen by the recruited ant is very close to that experienced in the case of a continuous deposition (see Fig. 2 of [25]). The key parameter is the dimensionless ratio $\delta = cd/D$ where c is the ant speed. The case $\delta \ll 1$ approaches the case of a continuous deposition. By contrast, in the opposite case $\delta \gg 1$, the diffusion is unable to wipe out the discontinuity of the deposition process. With the values $c \sim 1\,\mathrm{cm\,s^{-1}}$, $d \sim 0.1\,\mathrm{cm}$ and $D \sim 10^{-2}\,\mathrm{cm^2\,s^{-1}}$ (a value taken from [7], which might be slightly under-estimated), we find $\delta \sim 10$. This value is large, but still acceptable for the discontinuous deposition mechanism to form continuous odor trails under the influence of diffusion. In appendix 5, we illustrate this phenomenon by simulating discontinous pheromone deposition by a single ant. As can be seen on Fig. 12, pheromone diffusion leads to the appearance of a short trail.

For spots deposited at distances larger than 0.1 mm, another mechanism can be invoked. Indeed, from [26], it appears that the spots left by the ants are not strictly circular, but that they are elongated in the direction of motion. One can envision a mechanism by which the ant is able to sense the direction of motion of his partner through the sensing of one single deposition spot. Of course, the existence of such a mechanism is more speculative. But in this case, the osmotropotaxis mechanism invoked by [8, 9, 14] also breaks down and there exists no alternate theory or model.

We have run our model with parameters borrowed from [2] for *Lasius niger*. These parameters are in the last range (see section 3.1) and lead to a value $\delta = 10^4$ (with the same choice as above for the diffusion constant D). Still the model exhibits emergence of trails. And *Lasius niger* also does so! Of course, this does not indicate that the model captures the right phenomenology. To confirm or infirm the model assumptions, experiments able to test whether the ants are able to recover the orientation information from a single deposited spot would be needed.

3 Simulations and results

3.1 Choice of the modeling and numerical parameters

We use experimentally determined parameter values as often as possible. Since parameters are species-dependent, we focus on the species *Lasius niger*.

In our model, the motion of a single ant is described by three quantities: the speed c, the frequency of random velocity jumps λ_r and their amplitude σ. These three parameters have been estimated in different studies [4, 11] which give us a range of possible values. We choose rather low estimations of λ_r and σ (see Table 1) since in real experiments the estimation of these coefficients counts both for random jumps and recruitment by trails. The deposition rate of pheromone trails ν_d and their life time T_p have also been measured experimentally for *Lasius niger* [2]. After leaving a food source, an ant drops on the average .5 pheromone droplet per second. This experimental value gives us an upper bound for ν_d because it corresponds to an estimation of ν_d in a very specific situation where the ant activity level is high. In our simulations, we use $\nu_d = .2\,s^{-1}$. Since in our model, all the ants lay down pheromone particles, we also take a low estimation of the pheromone lifetime ($T_p = 100\,s$) otherwise the domain becomes saturated with pheromone particles.

By contrast, the ant-pheromone interaction has not been quantified experimentally. For this reason, we do not have experimental values for the pheromone detection radius R and the alignment probability per unit of time λ_p. In our simulations, we fix the radius of perception R equal to 1 cm (corresponding roughly to 2 body lengths). The alignment probability λ_p remains a free parameter in our model. By changing the value of λ_p, we can tune the influence of the pheromone-mediated interaction between the ants. A low value of λ_p corresponds to a weak interaction, whereas, for large values of λ_p, the ant velocities become controlled by the pheromone directions. In our simulations, λ_p varies from 0 to $3\,s^{-1}$.

For simplicity, all simulations are carried out in a square domain of size $L = 100$ cm with periodic boundary conditions. For the initial condition, 200 ants are randomly distributed in the domain. Their velocity ω_i is chosen uniformly on the circle $\mathbb{S}^1$. The ant-pheromone interaction is always taken non-polar unless otherwise stated.

We can estimate the average number of pheromone particles $\langle M \rangle$ at equilibrium, when the average is taken over realizations. The evolution of $\langle M \rangle(t)$ is given by the following differential equation:

$$\frac{d\langle M \rangle(t)}{dt} = \nu_d N - \frac{1}{T_p}\langle M \rangle(t),$$

where N is the number of ants, ν_d and T_p are (resp.) the pheromone deposition rate and lifetime. Thus, at equilibrium (i.e. $d\langle M \rangle/dt = 0$), the average number of

	Parameters	Value
L	Box size	100 cm
N	Number of ants	200
c	Ant speed	2 cm/s
λ_r	Random jump frequency	2 s^{-1}
σ	Random jump standard deviation	.1
ν_d	Pheromone deposition rate	.2 s^{-1}
T_p	Pheromone lifetime	100 s
R	Detection radius	1 cm
λ_p	Trail recruitment frequency	0-3 s^{-1}

Table 1: Table of the parameters used in the simulations.

pheromone particles is given by $\nu_d T_p N$. For our choice of parameters (Table 1), this corresponds to 4000 pheromone particles.

3.2 Detection of trails

3.2.1 Evidence of trail formation

The typical outcomes of the model are shown in figure 2. After an initial transient, we observe the formation of a network of trails. This network is not static, as we observe in the two graphics: the network at time $t = 2000\,s$ is significantly different from the network observed at time $t = 1000\,s$. Here, the goal is to provide statistical descriptors of this trail formation phenomenon and to analyze it.

3.2.2 Definition of a trail

To quantify the amount of particles that are organized into trails at a given time, we consider the collection of all particles, that is to say, the union of the sets of ants and of pheromone particles. Indeed collecting the pheromone particles allows us to trace back the recent history of the individuals. To define a trail, we fix two parameters: a distance $r_{\max}$ and an angle θ_{max}. We say that particle $P_i = (x_i, \omega_i)$ (P_i being either an ant or a pheromone particle) is *linked* to particle $P_j = (x_j, \omega_j)$ if the distance between the two particles is less than r_{max} and the angle between ω_i and ω_j is either less than θ_{max} or greater than $\pi - \theta_{max}$. In other words, we define a relationship (see figure 3):

$$P_i \sim P_j \quad \text{if and only if} \quad |x_i - x_j| < r_{max} \ \text{ and } \ |\sin(\omega_j - \omega_i)| < \sin\theta_{max}. \quad (3.1)$$

Using this relationship, particles can be sorted into different trails: we say that P and Q belong to the same *trail* if there exists particles $P_1, \ldots, P_k$ (*a path*) such

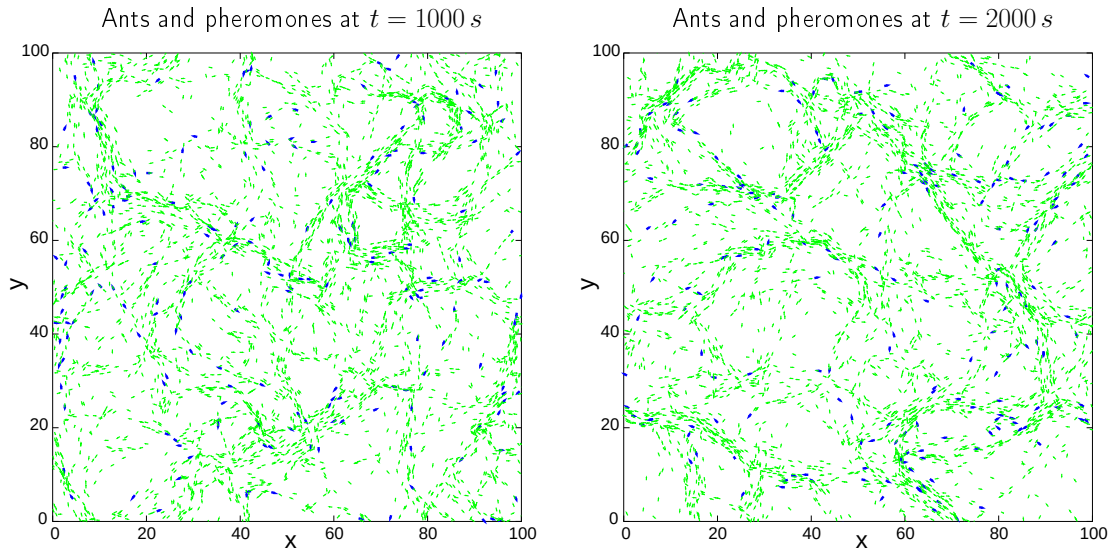


Figure 2: A typical output of the model at two different times. The ants are represented in blue and the pheromone particles in green. We clearly observe the formation of trails. Parameters of the simulation: $\lambda_p = 2s^{-1}$, $\Delta t = .05$ (see also Table 1).

that $P \sim P_1$, $P_1 \sim P_2, \ldots, P_k \sim Q$. Thus, a trail is defined as the connected components of the particles under the relationship (3.1). A trail is approximately a slowly turning lane of particles.

As a first example, in figure 4, we display the partitioning into trails of the previous simulations (figure 2) at time $t = 2000\,s$ with $r_{max} = 2$ cm and $\theta_{max} = 45°$. For these values, the largest trail (drawn in red in figure 4) consists of 2670 particles and the second largest (drawn in orange in figure 4) is made of 254 particles.

3.2.3 Statistics of the trails

We expect that trail formation results in the development of a small number of large trails, while unorganized states are characterized by a large number of small trails, most of them being reduced to single elements. Therefore, trail formation can be detected by observing the trail sizes. With this aim, we denote by $S_i(t)$ the size of the trail to which particle i belongs at time t. Let $\mathcal{N}(t)$ be the total number of particles, i.e. $\mathcal{N}(t) = N + \mathcal{P}(t)$ where N is the number of ants and $\mathcal{P}(t)$ is the number of pheromone particles at time t. We form

$$p_t(S) = \frac{|\{i \,|\, S_i(t) = S\}|}{\mathcal{N}(t)}, \quad S \in \mathbb{N}.$$

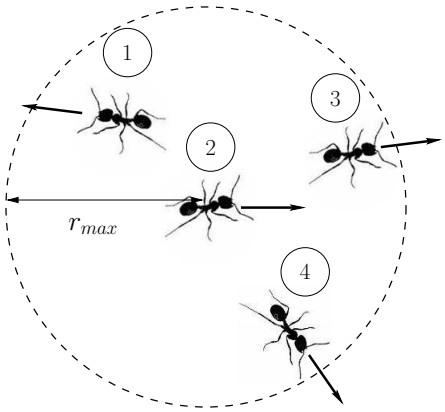


Figure 3: In this example, Ants 1, 2 and 3 are linked together: they form a *trail*. Ant 4 is not linked to Ant 2 since their directions are too different.

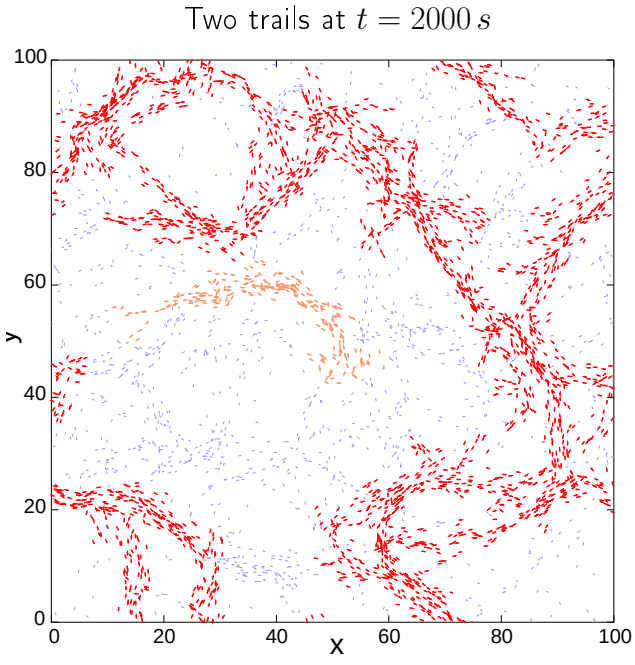


Figure 4: The two largest trails (drawn in red and orange) for the simulation depicted in figure 2 at time $t = 2000\,s$. Parameters for the estimation of the trails: $r_{max} = 2$ cm and $\theta_{max} = 45°$.

$p_t(S)$ is the probability that a particle belongs to a trail of size S at time t. An unorganized state is therefore characterized by a quickly decaying $p_t(S)$ as a function of S while a state where the particles are highly organized into trails displays a bimodal $p_t(S)$ with high values for large values of S. To display the distribution of $p_t(S)$ is easy: it is nothing but the histogram of the trail sizes S_i, collected from several independent simulations with identical parameters.

As an illustration, we provide the distribution $p_t(S)$ for the set parameters used to generate Figs. 2 and 4, (i.e. $\lambda_p = 2\,s^{-1}$, $r_{max} = 2$ cm and $\theta_{max} = 45°$), with 1000 realizations. We clearly observe in Fig. 5 (left) that the distribution $p_t(S)$ is bimodal: a first maximum is observed near the minimal value of S, i.e. $S = 1$, and a second maximum is observed near the values $S \approx 2500$. This indicates that a particle (representing either an ant or a pheromone) belongs to either a small-size trail ($S < 100$) or to a large-size trail ($S \approx 2500$). As a control sample for our statistical measurement, we run the same simulations but cutting off the ant-pheromone interaction (i.e. $\lambda_p = 0$) and proceed to the same analysis. In Fig. 5 (right), we observe that without the ant-pheromone interaction (blue histogram) the probability $p_t(s)$ is only concentrated near the value $S = 1$ and decays very fast to almost vanish for $S > 500$.

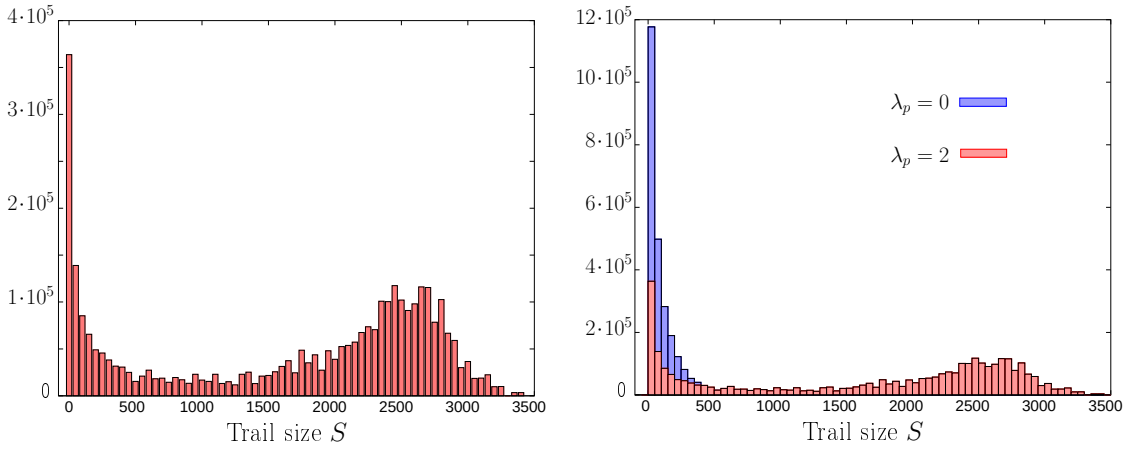


Figure 5: (**Left**) Histogram of the trail sizes S estimated from 1000 realizations. (**Right**) Histograms of S with and without ant-pheromone interaction ($\lambda_p = 2$ and $\lambda_p = 0$ resp.). The parameters for this simulation are the same as in Figs. 2 and 4.

3.3 Trail size

As observed in figure 5, ant-pheromone interactions lead to the formation of trails which are evidenced by the transformation of the shape of the distribution $p_t(S)$.

To perform a systematic parametric analysis of the trail formation phenomenon, we use the mean $\langle S \rangle$ of the distribution S:

$$\langle S \rangle = \sum_{S \in \mathbb{N}} S \, p_t(S).$$

The quantity $\langle S \rangle$ quantifies the level of organization of the system into trails. Indeed, large values of $\langle S \rangle$ indicate a high level of organization into trails while smaller values of $\langle S \rangle$ are the signature of a disordered system. For example, in Fig. 5, we have $\langle S \rangle = 1333.7$ when the ant-pheromone interaction is on with interaction frequency $\lambda_p = 2$. By contrast, its value falls down to $\langle S \rangle = 76.8$ when the ant-pheromone interaction is turned off (i.e. $\lambda_p = 0$) and the system is in a fully disordered state.

Our first use of the mean trail size $\langle S \rangle$ is to show that it stabilizes to a fixed value after an initial transient. Fig 6 shows the mean trail size $\langle S \rangle(t)$ for one simulation (dashed line) and averaged over 1000 different simulations (solid line). It appears that, after some transient, $\langle S \rangle(t)$ presents a lot of fluctuations about an averaged value. If the simulation is reproduced a large number of times and the mean trail size $\langle S \rangle(t)$ is averaged over all these realizations, the convergence towards a constant value becomes apparent.

Therefore, statistical analysis of the trail patterns using the mean trail size $\langle S \rangle$ become significant only once this constant value has been reached. In the forthcoming sections, analysis will be performed for simulation times equal to 2000 s, which is significantly larger than the time needed for the stabilization of $\langle S \rangle$ (about 800 s).

3.4 Evidence of a phase transition

In Fig. 7, we display $\langle S \rangle$ as a function of λ_p. For each value of λ_p, we estimate $\langle S \rangle$ by averaging it over 1000 independent simulations. We observe an increase of $\langle S \rangle$ when λ_p varies from 0 to 1 which means that a transition from an unorganized system to a system organized into trails arises. For larger values of λ_p, the influence of the ant-pheromone interaction saturates and $\langle S \rangle$ reaches a plateau at the approximate value $\langle S \rangle \approx 1300$. We also observe that this phase transition is smoother than phase transitions in thermodynamical systems. This may be due to the difficulty of quantifying what a 'network order' is. It is a possible that a different choice for the order parameter would reveal a sharper transition.

The transition from disorder to trails also depends on the other parameters of the model. For example, if we increase the noise by increasing the random jump frequency λ_r, the corresponding value of $\langle S \rangle$ decreases. In order to restore the previous value of $\langle S \rangle$ the ant-pheromone interaction frequency λ_p must be increased simultaneously. In Fig. 8, we plot $\langle S \rangle$ as a function of both the random jump

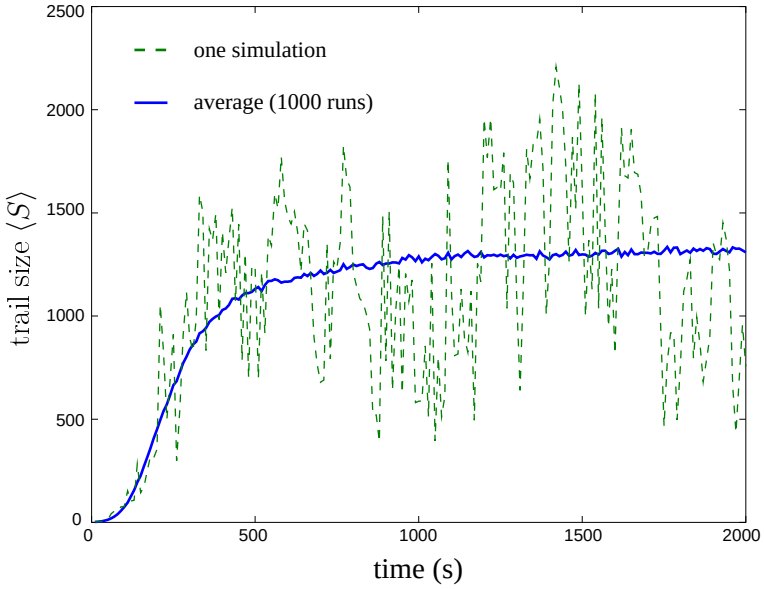


Figure 6: Mean trail size $\langle S \rangle$ as a function of time for one simulation (dashed line) and averaged over 1000 different simulations (solid line).

frequency λ_r and the ant-pheromone interaction frequency λ_p. We estimate $\langle S \rangle$ by averaging it over 100 realizations for each value of the pair (λ_p, λ_r). We still observe the transition from an unorganized state ($\langle S \rangle < 100$) to a state organized into trails ($\langle S \rangle \geq 1000$) when λ_p increases. However, as the noise λ_r increases, this transition becomes smoother. Moreover, $< S >$ still reaches values between 1300 and 1500 when λ_p is large for all values of λ_r but these values of $< S >$ are only attained at higher values of λ_p when λ_r is large.

At the value $\lambda_r = 0$, the transition from disorder ($\langle S \rangle \leq 100$) to trail-like organization ($\langle S \rangle \geq 1000$) is the fastest. However, the plateau reached by $\langle S \rangle$ when λ_p is large is significantly lower than for larger values of λ_r ($\langle S \rangle \approx 1000$ instead of 1300). This could be attributed to the fact that, without random jumps, the level of diffusion is too low, the ants do not mix enough, and trails have little opportunities to merge.

On the other hand, we can look for another explanation of this paradoxical lower value of $\langle S \rangle$ when λ_r is very small. Indeed, we notice that, in this case, the formed trails are much narrower than for larger values of λ_r. Fig. 9 (left) shows a simulation result using a quite small random jump frequency of $\lambda_r = .2$. We observe that the trails are narrower and more straight than those obtained with the larger value $\lambda_r = 2$ (figure 2). We can quantify statistically this feature by changing the parameters of trail detection r_{max} and θ_{max}. We reduce the maximum distance ($r_{max} = 1.5$ cm) and the maximum angle ($\theta_{max} = 35°$). With these smaller values,

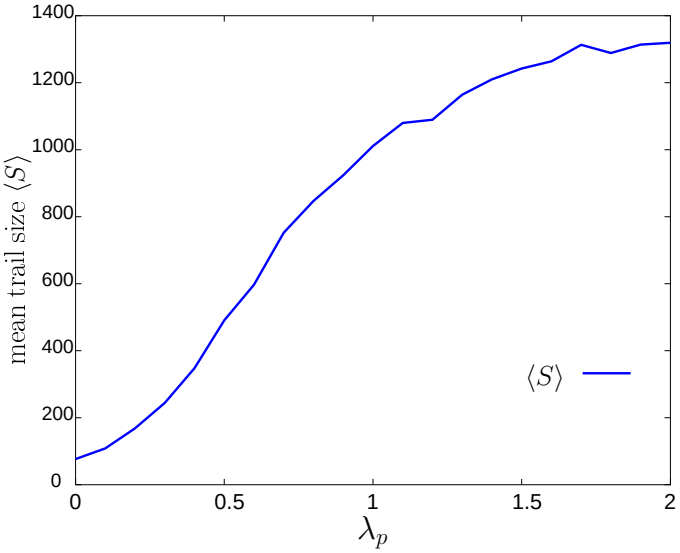


Figure 7: The mean $\langle S \rangle$ of the distribution $p_t(s)$ as a function of the ant-pheromone interaction frequency λ_p for a fixed value of the random jump frequency λ_r. Apart from λ_p, all parameter values are those given by Table 1.

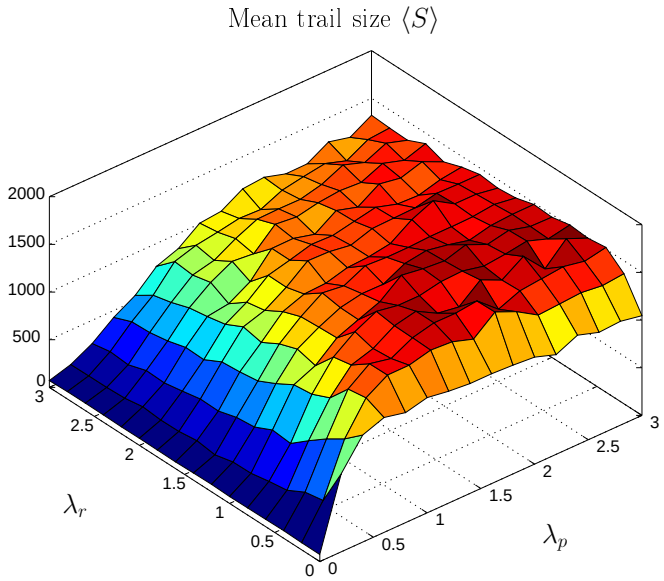


Figure 8: The mean $\langle S \rangle$ of the distribution $p_t(s)$ as a function of the pair (λ_r, λ_p), The cross-sections of this surface at a fixed value of λ_r shows the same behavior as in figure 7. Apart from λ_p and λ_r, all parameter values are those given by Table 1.

two particles are less likely to be connected. Then we proceed to the same analysis as in figure 8, by estimating the mean size of the trails $\langle S \rangle$ as a function of λ_r and λ_p, averaged over 100 realizations. As we observe in figure 9 (right), the mean size of the trails $\langle S \rangle$ is much larger for smaller values of λ_r and we recover the same behavior as that observed for larger values of λ_r. This illustrates the difficulty of working with an estimator which depends on arbitrary choices of scales (here the space and angular threshold of trail detection). A discussion of the dependence of the trail width upon the biological parameters is developed in the next section.

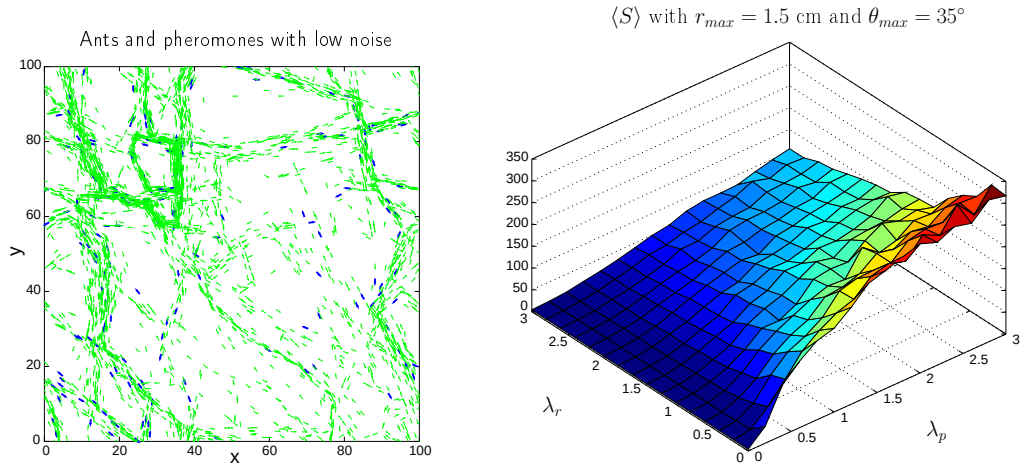


Figure 9: (**Left**) A simulation with low noise ($\lambda_r = .2$); the other parameters are the same as in figure 2 ($t = 2000\,s$). (**Right**) The mean size of the trails $\langle S \rangle$ estimated with $r_{max} = 1.5$ cm and $\theta_{max} = 35°$.

3.5 Trail width

A way to highlight the dependence of the trail width upon the model parameters is to compute a two-particle correlation distribution. Let a particle (be it an ant or a pheromone particle) i be located at position x_i and velocity ω_i. Denote by $\omega_i^\perp$ the orthogonal vector to ω_i in the direct orientation. For all particles $j \neq i$, we form the vector

$$X_{ij} = \begin{pmatrix} (x_j - x_i) \cdot \omega_i^\perp \\ (x_j - x_i) \cdot \omega_i \end{pmatrix}.$$

The distribution $\frac{2}{\mathcal{N}(\mathcal{N}-1)} f_2(X)$, with

$$f_2(X) = f_2(X_x, X_y) = \sum_{(i,j),\, i \neq j} \delta(X - X_{ij}),$$

where δ is the Dirac delta, provides the probability that, given a first particle (located at say x_0 with orientation ω_0), a second particle lies at location $x_0+\omega_0^\perp X_x+\omega_0 X_y$ (see figure 10 (left) for an illustration of the construction of f_2). Looking at this 2-particle density, trails appear as concentrations near a line passing through the origin and directed in the y-direction. Figure 10 (right) provides a histogram of the two-particle density f_2 for the simulation corresponding to the right picture of fig. 2. The above mentioned concentration is clearly visible. Additionally, the typical width of this concentration gives access to the typical width of the trails.

In order to better estimate the typical width of the trails, we plot cross-sections of the two-particle density f_2 along the line $\{y = 0\}$ (see figure 10). In practice, these cross-sections are determined by computing the following density

$$\bar{f}_2(r) = \sum_{(i,j),\, i\neq j,\, |(X_{ij})_y|\leq \xi} \delta(r - |(X_{ij})_x|).$$

where ξ is suitable chosen (of the order of 1 cm). Figure 11 (left) displays $\bar{f}_2(r)$ as a function of r for different values of the trail recruitment frequency λ_p and a fixed value of the random jump frequency equal to $\lambda_r = 2\ \mathrm{s}^{-1}$. It appears that $\bar{f}_2$ is higher and decreases faster for larger values of λ_p. The decay of $\bar{f}_2$ can give an estimate of the width of the trail: if we approximate the decay of $\bar{f}_2$ by an exponential,

$$\bar{f}_2(r) \approx f_0 \exp\left(-\frac{r}{r_0}\right) \qquad \text{for} \quad r \approx 0,$$

then r_0 measures the typical width of the trail. This quantity can be estimated using the formula:

$$r_0 = \frac{1}{|(\ln \bar{f}_2)'(0)|}. \tag{3.2}$$

As we observe in Table 2, the width r_0 increases as λ_p decreases. Therefore, increasing the trail recruitment frequency increases the intensity of the particles interactions and produces trails with smaller width. Figure 11 (right) displays $\bar{f}_2(r)$ as a function of r for different values of the random jump frequency λ_r and a fixed value of the trail recruitment frequency equal to $\lambda_p = 2\ \mathrm{s}^{-1}$. Here, the trail width r_0 estimated from $\bar{f}_2$ is larger for large values of λ_r (see Table 2), indicating that the typical width of the trails increases with increasing λ_r, as it should.

We also observe a discontinuity at $r = 0$ for all the functions $\bar{f}_2$ (figure 11). These jumps are easily explained by the deposit process: each time an ant drops a pheromone particle, the new pheromone particle and the ant are located at the same position exactly. This results in a peak of concentration of $\bar{f}_2$ at $r = 0$.

3.6 Discussion and comparison with previous works

We compare our approach with the models of Edelstein-Keshet and coworkers [18, 20, 48] on the one hand, and of Rauch et al [40] on the other hand. We recall that

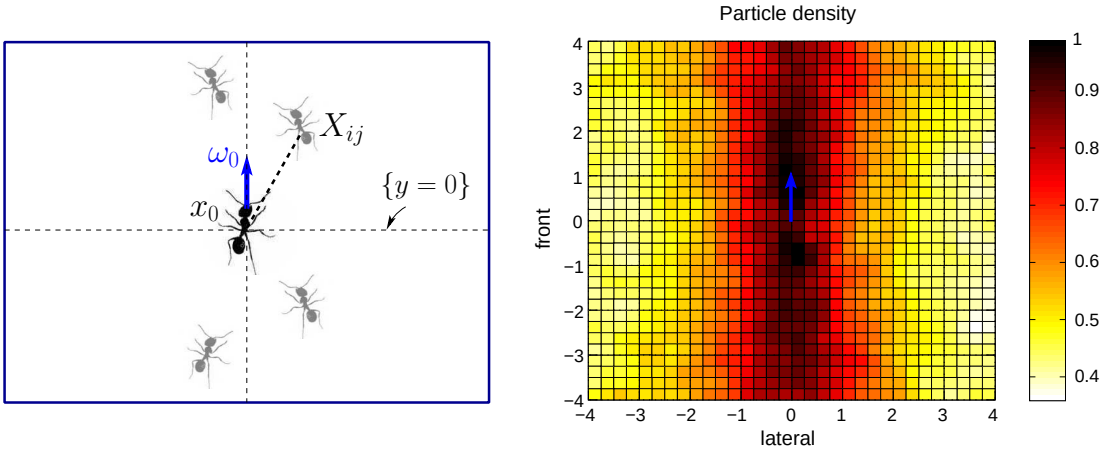


Figure 10: (**Left**) Construction of the two-particle distribution f_2. (**Right**) Histogram of the two-particle density f_2 for the test-case corresponding to the right picture of fig. 2. $f_2(X)$ is represented via a color scale as a function of the two components of X.

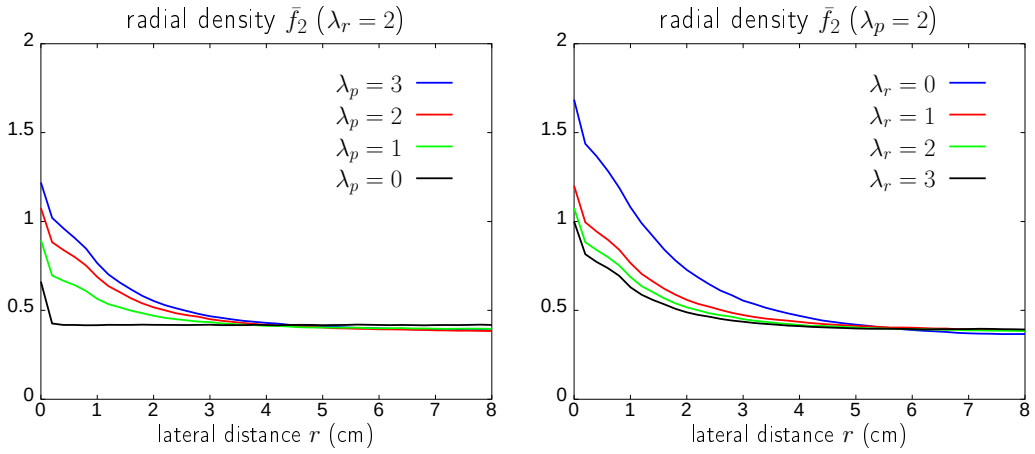


Figure 11: (**Left**) $\bar{f}_2(r)$ as a function of r for different values of the trail recruitment frequency λ_p and a fixed value of the random jump frequency equal to $\lambda_r = 2$ s^{-1}. (**Right**) $\bar{f}_2(r)$ as a function of r for different values of the random jump frequency λ_r and a fixed value of the trail recruitment frequency equal to $\lambda_p = 2$ s^{-1}.

λ_p	r_0 (cm)
3	2.796
2	3.181
1	4.350

λ_r	r_0 (cm)
0	2.532
1	2.964
2	3.181
3	3.345

Table 2: Estimations of the width r_0 (3.2) of the trails using $\bar{f}_2$ given in figure 11. We estimate the derivative of $\ln \bar{f}_2(r)$ near 0 using the values of r between .1 and 2.

both models are Cellular Automata posed on a square lattice. While the former relies on a probabilistic mechanism for trail recruitment, the latter uses a physical force description in terms of an 'osmotropotaxis potential' depending of the local pheromone density. Both models include pheromone decay and random jumps. By contrast, the discrete model of Deneubourg et al [15] does not include pheromone decay. The mean-field model of Vincent et al [46] investigates the effect of a non-isotropic turning kernel while the active walker models of [41] and [44] includes two distinct species of pheromones. The consideration of these two effects is beyond the scope of the present paper.

One of the motivations for introducing the present model was to investigate whether the square lattice geometry could influence the trail network pattern. Inspection of [48], Fig. 5 or [40], Fig. 1 leads to the observation that the trail patterns organize themselves preferentially along the diagonals of the square domain. There is a striking geometric effect which is probably due to the bias introduced by the constrained motion on a square lattice. By contrast, our model does not exhibit such a bias and the distribution of orientations of trails spans continuously all the possible directions (see e.g. Fig 2 or Fig. 4).

The trails formed in [48] or [40] are very thin (one cell wide), while the trails formed by our model have variable widths. The average trail width in our model can be tuned by changing the parameters, such as the trail recruitment or random jump frequencies. By contrast, the tuning of these parameters in [48], changes the network topology but not the width of the trails. They remain very narrow. The fidelity in [48] characterizes the propensity of ants to follow trails and corresponds to the inverse of the random jump frequency in our model. In the latter, when the fidelity is increased, the width of the trail is decreased (see table 2, right). Such an effect does not appear in the former. In [40], the role of the fidelity is played by the osmotropotaxis sensitivity. In this model, there is a finite range of osmotropotaxis sensitivities where trail networks are formed. For weak sensitivities no particular pattern is formed, but for large sensitivities, particles aggregate into patches in a fashion similar to chemotaxis phenomena, rather than forming trails. No such effect is observed in our model where the quality of the trails, both in width and size is

increased by reducing the random jump frequency.

In [48], the transition from disordered motion to network order when the fidelity is increased is very abrupt. The mean length of trail followed by an individual is multiplied by a factor 4 when the fidelity is increased by only 3% around a critical value. In [40], this phase transition (when the osmotropotaxis sensitivity is increased) is less abrupt. The qualitative features of this phase transition can be graphically inferred from Fig. 2 of [40]. The phase transition occurs when the osmotropotaxis sensitivity is changed within a range of about 50% of the critical value of the osmotropotaxis sensitivity (a bit more or less depending on the value of the sensory capacity, which is a parameter allowing for a saturation of the trail recruitment frequency when the pheromone density is large). From section 3.4 and Figs. 7, and 8, the width of the phase transition in our model is comparable to what is found in [40]. In our case, the larger width of the phase transition as compared to [48] may be associated to the performances of the model in terms of network plasticity (see below). Since the transition from disorder to network order is less abrupt, there is room for an intermittency behavior which may favor network topology and geometry changes over time.

In [18], the trail network seems to evolve by maintaining the formed trails and increasing the network complexity. The time sequence displayed in [18], Fig. 5 shows two main trails (which coincide with the diagonals of the square). These main trails are kept once formed and support secondary branches with increasing branching complexity as time proceeds. A similar conclusion can be drawn from Fig. 1 of [40] where the main trail appears around $t = 412$ and is kept until $t = 1753$. By contrast, the two time snapshots provided in Fig. 2 (left and right and which are taken at $t = 1000$ and $t = 2000$ respectively) reveal that our model does not favor the maintenance over time of the trail network (in both our work and in [40], the particles were initially randomly distributed in position and velocity). The features shown by the left and right pictures of Fig. 2 are qualitatively similar but very different in the details. Therefore, our model enables network plasticity over time, as anticipated.

As a conclusion, the present model offers more realistic features in terms of network geometry and network plasticity compared with previous work. As a counter part, the phase transition from disorder to network order when the fidelity to trails is increased is less abrupt, but this smoother phase transition may be associated with the larger plasticity of the formed network.

4 Kinetic and continuum descriptions

4.1 Framework

In this section, we propose meso- and macro-scopic descriptions of the previously discussed ant dynamics. We first propose a kinetic model, i.e. a model for the probability distributions of ants and of pheromone particles. The derivation of this kinetic model is formal and based on analogies with the underlying discrete dynamics. A rigorous derivation of the kinetic model from the discrete dynamics has not yet been accomplished. Issues such as the validity of the chaos propagation property [12], which is the key for proving such results, may be quite difficult to solve. Then, fluid limits of this kinetic model will be considered. We will notice that the resulting fluid models can only exhibit the development of trails if some amplification mechanism is incorporated. Here, we will consider that the ants choose the stronger trails with a higher probability than the weaker ones. By contrast, the numerical simulations above indicate that such a mechanism is not needed to produce emerging trails at the level of the Individual-Based Model. This is probably because, in the absence of any amplification mechanism, some stochasticity is needed. In the macroscopic model, all sources of stochasticity have been averaged out.

4.2 Kinetic model

In this section, we introduce the kinetic model of the discrete ant-pheromone interaction on a purely formal basis. We introduce the ant distribution function $F(x, \omega, t)$ and the pheromone particle distribution function $G(x, \omega, t)$, for $x \in \mathbb{R}^2$, $\omega \in \mathbb{S}^1$ and $t \geq 0$. They are respectively the number density in phase-space (x, ω) of the ants (respectively of the pheromone particles), i.e. the number of such particles located at position x with orientation ω at time t. Here, we remark that the consideration of directed pheromone particles requires the introduction of a pheromone density in (position, orientation) phase-space in the same manner as for the ants.

Trail dynamics. The trail dynamics is described by the ordinary differential equation:

$$\partial_t G(x, \omega, t) = \nu_d F(x, \omega, t) - \nu_e G(x, \omega, t), \tag{4.1}$$

This equation can be easily deduced from the evolution of the probability density of the underlying stochastic Poisson process. The first term describes deposition by the ants according to a Poisson process of frequency ν_d while the second term results from the finite lifetime expectancy $T_p = \nu_e^{-1}$ of the pheromone particles. Pheromone particles are assumed immobile, which explains the absence of any convection or diffusion operator in this model. Discarding pheromone diffusion is done

for simplicity only and can be easily added. It would add a term $\Delta_x G$ or $\Delta_\omega G$ at the right-hand side of (4.1) according to whether one considers spatial or orientational diffusion.

Ant dynamics. The ant distribution function is governed by the following kinetic equation:

$$\partial_t F + c\,\omega \cdot \nabla_x F = Q(F). \tag{4.2}$$

The left-hand side describes the ant motion with constant speed c in the direction ω. The right hand side is a Boltzmann-type operator which describes the rate of change of the distribution function due to the velocity jump processes. Q is decomposed into

$$Q = Q_r + Q_p,$$

where Q_r and Q_p respectively describe the random velocity jumps and the trail recruitment jumps.

Both operators $Q_k(x,\omega,t)$, $k = p$ or r express the balance between gain and loss due to velocity jumps, i.e. $Q_k(x,\omega,t) = Q_k^+ - Q_k^-$. The gain term Q_k^+ describes the rate of increase of $F(x,\omega,t)$ due to particles which have post-jump velocity ω and pre-jump velocity ω'. Similarly, the loss term Q_k^- describes the rate of decay of $F(x,\omega,t)$ due to particles jumping from ω to another velocity ω'. The jump probability $P_k(\omega \to \omega')d\omega'$ is the probability per unit time that a particle with velocity ω jumps to the neighborhood $d\omega'$ of ω' due to jump process k. Therefore, the expression of Q_k is:

$$Q_k(F)(x,\omega,t) = \int_{\mathbb{S}^1} \Big(P_k(\omega' \to \omega)F(x,\omega',t) - P_k(\omega \to \omega')F(x,\omega,t)\Big)d\omega'. \tag{4.3}$$

where the positive term corresponds to gain and the second term, to loss. By symmetry, we note that

$$\int_{\mathbb{S}^1} Q_k(F)(x,\omega,t)\,d\omega = 0, \tag{4.4}$$

for any distribution F. This expresses that the local number density of particles is preserved by the velocity jump process.

Now we describe the expressions of the jump probabilities P_k. For both processes, we postulate the existence of a detailed balance principle, which means that the ratio of the direct and inverse collision probabilities are equal to the ratios of the corresponding equilibrium probabilities

$$\frac{P_k(\omega' \to \omega)}{P_k(\omega \to \omega')} = \frac{h_k(\omega)}{h_k(\omega')}, \tag{4.5}$$

where h_k is the equilibrium probability of the process k ($k = r$ or $k = p$). Using (4.5), we can define:

$$\Phi_k(\omega',\omega) = \frac{1}{h_k(\omega)}P_k(\omega' \to \omega) = \Phi_k(\omega,\omega'),$$

which is symmetric by exchange of ω and ω' and write

$$Q_k(F)(x,\omega,t) = \int_{\mathbb{S}^1} \Phi_k(\omega,\omega')\Big(h_k(\omega)\,F(x,\omega',t) - h_k(\omega')\,F(x,\omega,t)\Big)d\omega'. \qquad (4.6)$$

From this equation, it is classically deduced that the equilibria, i.e. the solutions of $Q_k(F) = 0$ are given by $F(x,\omega,t) = \rho(x,t)h_k(\omega)$ with arbitrary ρ. We recall the argument here for the sake of completeness. Indeed, such F are clearly equilibria. Reciprocally, if F is an equilibrium, then, using the symmetry of Φ_k leads to

$$\begin{aligned} 0 &= \int_{\mathbb{S}^1} Q_k(F)\,\frac{F}{h_k}\,d\omega \\ &= -\frac{1}{2}\int_{(\mathbb{S}^1)^2} \Phi_k(\omega,\omega')\,h_k(\omega)\,h_k(\omega')\,\left(\frac{F(x,\omega',t)}{h_k(\omega')} - \frac{F(x,\omega,t)}{h_k(\omega)}\right)^2 d\omega\,d\omega'. \end{aligned}$$

The last expression is the integral of a non-negative function which therefore must be identically zero for any choice of (ω,ω'). It follows that the only equilibria are functions of the form ρh_k with ρ only depending on (x,t). It is not clear if the biological processes actually do satisfy the detailed balance property but this hypothesis simplifies the discussion. Indeed, with this assumption, the equilibria h_k and the jump probabilities Φ_k can be specified independently.

Trail recruitment jumps. For trail recruitment, we first need to specify the equilibrium distribution as a function of the pheromone distribution. Several options are possible: non-local interactions, local ones, preferential choice, non-polar interactions.

1. Non-local interaction. We first introduce the sensing application:

$$S_R(x,\omega,t) = \frac{1}{\pi R^2}\int_{|x-y|<R} G(y,\omega,t)dy,$$

where R represents the perception radius of the ant, i.e. the maximal distance at which it can feel deposited pheromone particles. The quantity $S_R(x,\omega,t)$ represents the density of pheromone particles pointing towards ω which can be perceived by an ant at point x in its perception area. We also define

$$T_R(x,t) = \int_{\mathbb{S}^1} S_R(x,\omega,t)\,d\omega,$$

the pheromone particle total density within the perception radius, regardless of orientation. Then, we let the equilibrium distribution of the trail recruitment process as follows:

$$h_p(\omega) = g_R(x,\omega,t) := \frac{S_R(x,\omega,t)}{T_R(x,t)}, \qquad (4.7)$$

which, by construction, is a probability density. Now, the expression for the transition probability reads:

$$\Phi_p(\omega \to \omega'; x, t) = \lambda_p \gamma(T_R(x,t))\phi_p(\omega \cdot \omega'), \tag{4.8}$$

where λ_p is the trail-recruitment frequency and γ is a dimensionless increasing function of T which accounts for the fact that recruitment by trails increases with pheromone particle density (in the discrete particle dynamics, we have taken $\gamma(T) = \pi R^2 T$, the total number of pheromone particles in the sensing region). The function $\phi_p(\omega \cdot \omega')$ represents the angular dependence of the interaction process and is such that

$$\frac{1}{2\pi}\int_{\mathbb{S}^1} \phi_p(\omega \cdot \omega')\, d\omega' = 1. \tag{4.9}$$

We assume that it is independent of the pheromone distribution for simplicity. Inserting (4.8) into (4.6), the trail-recruitment operator is written:

$$Q_p(F)(x,\omega,t) = \lambda_p \gamma(T_R(x,t)) \int_{\mathbb{S}^1} \phi_p(\omega \cdot \omega')(g_R(\omega)\, F(x,\omega',t) - g_R(\omega')\, F(x,\omega,t))d\omega'. \tag{4.10}$$

The choice of ϕ_p which corresponds to the discrete dynamics discussed in the previous sections is $\phi_p(\omega \cdot \omega') = 1$. Inserting this prescription into (4.10) and using (4.7) leads to the simplified operator

$$Q_p(F)(x,\omega,t) = \lambda_p \gamma(T_R(x,t)) \left(\rho(x,t)\frac{S_R(x,\omega,t)}{T_R(x,t)} - F(x,\omega,t)\right),$$

with

$$\rho(x,t) = \int F(x,\omega,t) d\omega,$$

the local ant density at x.

2. Local interaction. This corresponds to taking the limit of the sensing radius to zero: $R \to 0$ which leads to

$$h_p(\omega) = g(\omega) := \frac{G(x,\omega,t)}{T(x,t)}, \quad T(x,t) = \int_{\mathbb{S}^1} G(x,\omega,t)\, d\omega.$$

T is the local trail density. Then, the expression of the collision operator is easily deduced from (4.10) by changing g_R into g. In the case where $\phi_p = 1$, we get the expression:

$$Q_p(F)(x,\omega,t) = \lambda_p \gamma(T(x,t))\left(\rho(x,t) g(x,\omega,t) - F(x,\omega,t)\right).$$

3. Preferential choice. We can envision a mechanism by which the ants can sense and choose the most frequently used trails. A possible way to model this preferential choice is by postulating an equilibrium distribution of the form

$$h_p(\omega) = g_R^{[k]}(\omega) = \frac{g_R^k(\omega)}{\int_{\mathbb{S}^1} g_R^k(\omega)\, d\omega}, \tag{4.11}$$

with a power $k > 1$. Indeed, it can be shown [6] that the maxima of $g_R^{[k]}$ are larger than those of g_R and similarly, the minima are lower. Additionally, the monotony is preserved, i.e.

$$g_R(\omega) \leq g_R(\omega') \Longrightarrow g_R^{[k]}(\omega) \leq g_R^{[k]}(\omega'), \quad \forall(\omega, \omega') \in (\mathbb{S}^1)^2.$$

Therefore, taking $g_R^{[k]}(\omega)$ as equilibrium distribution of the ant-pheromone interaction means that the ants choose the trails ω with a higher probability when the trail density in direction ω is high and with lower probability when the trail density is low. The expression of the collision operator is easily deduced from (4.10) by changing g_R into $g_R^{[k]}$. In the case where $\phi_p = 1$, we get:

$$Q_p(F)(x, \omega, t) = \lambda_p \gamma(T_R(x, t)) \left(\rho(x, t) g_R^{[k]}(x, \omega, t) - F(x, \omega, t)\right).$$

This mechanism can also be combined with a local interaction, by replacing g_R by the pheromone particle local angular probability g. We note that this mechanism is not implementable in the discrete dynamics because the operation $g \to g^{[k]}$ is only defined for measures g which belong to the Lebesgue space $L^k(\mathbb{S}^1)$. However, sums of Dirac deltas, which correspond to the measure g in the Individual-Based Model, do not belong to this space. Therefore, a smoothing procedure must be applied to such measures beforehand. Since, it is not possible to obtain experimental data about the smoothing procedure and the power k, the preferential choice model has not been used in the numerical experiments of the previous sections.

4. Non-polar interaction. The above described ant-pheromone interactions are polar ones, i.e. the pheromone particles are supposed to have both a direction and an orientation. However, we can easily propose a non-polar interaction, for which an ant of velocity ω chooses ω' among the pheromone particle directions and their opposite in such a way that the angle $\widehat{(\omega, \omega')}$ is acute, i.e. such that $\omega \cdot \omega' > 0$. For this purpose, we modify the equilibria of the trail recruitment operator as follows:

$$h_p(x, \omega, t) = g_R^{(sym)} := \frac{S_R(x, \omega, t) + S_R(x, -\omega, t)}{2T_R(x, t)},$$

and suppose that

$$\phi_p(\omega \cdot \omega') = 0, \quad \text{when } \omega \cdot \omega' \leq 0. \tag{4.12}$$

The expression of the collision operator is easily deduced from (4.10) by making the change of g_R into $g_R^{(sym)}$ and imposing the restriction (4.12). In the case where

$$\phi_p(\omega \cdot \omega') = 2H(\omega \cdot \omega'),$$

where H is the Heaviside function (i.e. the indicator function of the positive real line), we find

$$Q_p(F)(x,\omega,t) = \lambda_p \gamma(T_R(x,t)) \left[\frac{1}{T_R(x,t)} \left(\rho_\omega^+(x,t)\, S_R(x,\omega,t) + \right. \right. \\ \left. \left. + \rho_\omega^-(x,t)\, S_R(x,-\omega,t) \right) - F(x,\omega,t) \right],$$

with

$$\rho_\omega^\pm(x,t) = \int F(x,\omega',t)\, H(\pm\omega \cdot \omega')\, d\omega',$$

is the local density of ants pointing in a direction making respectively an acute angle (for ρ_ω^+) or obtuse angle (for ρ_ω^-) with ω at x.

Random velocity jumps. For random velocity jumps, we assume a uniform equilibrium

$$h_r(\omega) = \frac{1}{2\pi},$$

with a given jump probability

$$\Phi_r(\omega,\omega') = \lambda_r\, \phi_r(\omega,\omega').$$

Here, ϕ_r satisfies the same normalization condition (4.9) as the trail recruitment jump transition probability and λ_r is the random velocity jump frequency. With (4.6), we find the expression of Q_r:

$$Q_r(F) = \lambda_r \left(\int \phi_r(\omega.\omega') F(x,\omega',t) \frac{d\omega'}{2\pi} - F(x,\omega,t) \right).$$

If $\phi_r = 1$, then Q_r reduces to

$$Q_r(F) = \lambda_r \left(\frac{\rho(x,t)}{2\pi} - F(x,\omega,t) \right).$$

Summary of the kinetic model. Below, we collect all equations of the kinetic model. We have written the model in the framework of non-local interaction, preferential choice and non-polar interaction. The restriction to simpler rules is easily

deduced.

$$\partial_t G(x,\omega,t) = \nu_d F(x,\omega,t) - \nu_e G(x,\omega,t), \tag{4.13}$$

$$\partial_t F + c\,\omega\cdot\nabla_x F = Q_r(F) + Q_p(F), \tag{4.14}$$

$$Q_p(F)(x,\omega,t) = \lambda_p\gamma(T_R(x,t))\int_{\mathbb{S}^1}\phi_p(\omega,\omega')\Big(h_p(\omega)\,F(x,\omega',t) - h_p(\omega')\,F(x,\omega,t)\Big)d\omega', \tag{4.15}$$

$$Q_r(F)(x,\omega,t) = \lambda_r\int_{\mathbb{S}^1}\phi_r(\omega,\omega')\Big(F(x,\omega',t) - F(x,\omega,t)\Big)d\omega', \tag{4.16}$$

$$h_p(\omega) = (g_R^{(sym)})^{[k]}(\omega), \quad g_R^{(sym)}(x,\omega,t) = \frac{S_R(x,\omega,t) + S_R(x,-\omega,t)}{2T_R(x,t)}, \tag{4.17}$$

$$S_R(x,\omega,t) = \frac{1}{\pi R^2}\int_{|x-y|<R} G(y,\omega,t)dy, \quad T_R(x,t) = \int_{\mathbb{S}^1} S_R(x,\omega,t)\,d\omega. \tag{4.18}$$

In the following section, we consider fluid limits of the present kinetic model.

4.3 Macroscopic model

Scaling. In order to study the macroscopic limit of the kinetic model (4.13)-(4.18), we use the local interaction approximation $R = 0$, with polar interaction and uniform transition probabilities $\phi_r = 1$, $\phi_p = 1$. In this case, the model simplifies into

$$\partial_t G = \nu_d\,F - \nu_e\,G, \tag{4.19}$$

$$\partial_t F + c\,\omega\cdot\nabla_x F = Q_r(F) + Q_p(F), \tag{4.20}$$

$$Q_p(F) = \lambda_p\,\gamma(T)\;(\rho\,h - F)\,, \tag{4.21}$$

$$Q_r(F) = \lambda_r\,\left(\frac{\rho}{2\pi} - F\right), \tag{4.22}$$

$$h = g^{[k]}, \quad g = \frac{G}{T}, \quad T = \int_{\mathbb{S}^1} G\,d\omega, \quad \rho = \int_{\mathbb{S}^1} F\,d\omega, \tag{4.23}$$

where the meaning of the power $[k]$ operation has been defined at (4.11). We now change to dimensionless variables. We let t_0, x_0, ρ_0, T_0, be respectively units of time, space, ant density and pheromone particle density and we introduce $x' = x/x_0$, $t' = t/t_0$, $\rho' = \rho/\rho_0$, $T' = T/T_0$, $F' = F/\rho_0$, $G' = G/T_0$ as new variables and unknowns. Specifically, t_0 is chosen to be the macroscopic time scale (e.g. the observation time scale). Similarly, x_0 is the macroscopic length scale (e.g. the size of the experimental arena). We impose $x_0 = ct_0$, so that the time and space derivatives in (4.20) are of the same orders of magnitude. This scaling allows us to observe the system at the convection scale where the convection speed of the ant density is finite.

We introduce the following dimensionless parameters:

$$\bar{\nu}_d = \nu_d\, t_0, \quad \bar{\nu}_e = \nu_e\, t_0 \frac{T_0}{\rho_0}, \quad \bar{\lambda}_p = \lambda_p\, t_0, \quad \bar{\lambda}_r = \lambda_r\, t_0.$$

We make the assumption that the macroscopic time scale t_0 is very large compared to the microscopic time scales λ_r^{-1} and λ_p^{-1} which are both supposed to be of the same orders of magnitude. Indeed, during the time needed for patterns to develop, ants make a large number of jumps of either kind. Following this assumption, we introduce:

$$\varepsilon = \frac{1}{\bar{\lambda}_p} = \frac{1}{\lambda_p t_0} \ll 1, \quad \sigma = \frac{\bar{\lambda}_r}{\bar{\lambda}_p} = \frac{\lambda_r}{\lambda_p} = O(1).$$

Concerning the pheromone particle dynamics, we assume that $\bar{\nu}_d$ and $\bar{\nu}_e$ are of the same orders of magnitude, which amounts to supposing that pheromone deposition and evaporation balance each other. Indeed, if one of these two antagonist phenomena predominates, then, after some transient the pheromone particle density will become either too low or too large and we cannot expect any interesting patterns to emerge in this case. We introduce

$$\eta = \frac{1}{\bar{\nu}_d} = \frac{1}{\nu_d\, t_0}, \quad \kappa = \frac{\bar{\nu}_e}{\bar{\nu}_d} = \frac{\nu_e}{\nu_d} = O(1).$$

In what follows, we will assume that $\eta = O(1)$ i.e. that the pheromone dynamics occurs at the macroscopic time scale.

After rescaling, system (4.19)-(4.23) becomes (where we drop the primes for the sake of clarity, and we highlight the dependence of the unknowns F and G upon the scaling parameter ε by writing F^ε and G^ε):

$$\eta\, \partial_t G^\varepsilon = F^\varepsilon - \kappa\, G^\varepsilon, \tag{4.24}$$

$$\varepsilon\, (\partial_t F^\varepsilon + \omega \cdot \nabla_x F^\varepsilon) = Q(F^\varepsilon), \tag{4.25}$$

with the collision operator $Q = Q_r + Q_p$ given by

$$Q(F) = (Q_r + Q_p)(F) = (\gamma(T) + \sigma)\, (\mu\, \rho - F), \tag{4.26}$$

$$\mu = \frac{\gamma(T) h + \frac{\sigma}{2\pi}}{\gamma(T) + \sigma}, \quad h = g^{[k]}, \quad g = \frac{G}{T}, \tag{4.27}$$

$$T = \int_{\mathbb{S}^1} G\, d\omega, \quad \rho = \int_{\mathbb{S}^1} F\, d\omega. \tag{4.28}$$

Macroscopic limit $\varepsilon \to 0$ of the kinetic model (4.24)-(4.28). Here, we suppose that $\eta = O(1)$ i.e. we assume that the pheromone dynamics occurs at the macroscopic scale. We show that the limit $\varepsilon \to 0$ of (4.24)-(4.28) consists of the

following system for the ant density $\rho(x,t)$, pheromone particle density $T(x,t)$ and pheromone distribution function $g(x,\omega,t)$:

$$\partial_t \rho + \nabla_x \cdot \left(\frac{\gamma(T)}{\gamma(T)+\sigma}\, j_h \right) = 0., \tag{4.29}$$

$$\eta \partial_t T = \rho - \kappa T, \tag{4.30}$$

$$\eta \partial_t g = \frac{\rho}{T} \left(\frac{\gamma(T) g^{[k]} + \frac{\sigma}{2\pi}}{\gamma(T)+\sigma} - g \right), \tag{4.31}$$

with $h = g^{[k]}$ and where $j_\varphi = \int_{\mathbb{S}^1} \varphi(\omega)\, \omega \, d\omega$, denotes the flux of any function $\varphi(\omega)$. Eq. (4.31) is a closed equation for g. Once g is determined and inserted into (4.29) the evolution of the ant density ρ can be computed. The ant distribution function f is equal to μ at any time, with μ given by (4.27).

Indeed, in this limit, supposing that $F^\varepsilon \to F$, we get $Q(F) = 0$ from (4.25). Therefore, from (4.26), we obtain

$$F = \rho\mu, \qquad \text{or} \qquad f = \mu. \tag{4.32}$$

The equation for $\rho(x,t)$ is obtained by integrating (4.25) with respect to ω and using (4.4). We find:

$$\partial_t \rho + \nabla_x \cdot j_F = 0.$$

Remarking that $j_F = \rho j_\mu$ and that the flux of the isotropic distribution vanishes, we finally get from (4.27):

$$j_\mu = \frac{\gamma(T)}{\gamma(T)+\sigma}\, j_h, \tag{4.33}$$

and consequently, ρ satisfies (4.29). To compute the pheromone distribution function g, we integrate (4.24) with respect to ω and get (4.30). Then, combining (4.30) with (4.24), we deduce that

$$\eta \partial_t g = \frac{\rho}{T}(f - g). \tag{4.34}$$

But, with (4.32) and (4.27), we deduce that g satisfies (4.31).

Some comments are now in order. In the limit $\varepsilon \to 0$ the ant distribution function instantaneously relaxes to the distribution μ. This distribution reflects the antagonist effects of trail recruitment and random velocity jumps. Indeed, μ is the convex combination of the equilibrium distributions h and $\frac{1}{2\pi}$ of the two processes respectively. The weights, respectively equal to $\gamma(T)/(\gamma(T)+\sigma)$ and $\sigma/(\gamma(T)+\sigma)$ show that the influence of the trail recruitment process is more pronounced at large pheromone densities, since γ increases with T. On the other hand, if the frequency of random jump σ is increased, the trail recruitment process is comparatively less important.

Case $k = 1$: no preferential choice. If the ants do not implement a preferential choice of the largest trails, i.e. if $k = 1$, eq. (4.31) simplifies into

$$\eta \partial_t g = \frac{\rho}{T} \frac{\sigma}{\gamma(T) + \sigma} \left(\frac{1}{2\pi} - g \right). \tag{4.35}$$

This is a classical relaxation equation of g towards the isotropic distribution $\frac{1}{2\pi}$. As a consequence, in this case, there is no trail formation and the large time behavior of the system leads to a homogeneous steady state. This description can be complemented by looking at the pheromone flux j_g. The term 'flux' is chosen by analogy with the expression of the ant flux. Note however that pheromone particles do not move and that j_g is rather a measure of the local orientational order of the pheromone particles. The associated order parameter is the quantity $\alpha = |j_g|/T$ which is comprised between 0 and 1. The case $\alpha = 0$ corresponds to local total disorder while the case $\alpha = 1$ correspond to local complete alignment. Now, (4.35) leads to

$$\eta \partial_t j_g = -\frac{\rho}{T} \frac{\sigma}{\gamma(T) + \sigma} j_g.$$

As a consequence, the direction of the local pheromone flux never changes and its intensity decays to 0 as $t \to \infty$. Additionally, eq. (4.33) which in the case $k = 1$ gives $j_\mu = \frac{\gamma(T)}{\gamma(T)+\sigma} j_g$ shows that the ant flux is always proportional to and smaller than the pheromone flux. Therefore, it also converges to 0 for large times. Note that this direction may not correspond to the maximum of the pheromone distribution g. Therefore, the ant flux may not be aligned with any particular trail, defined as such a maximum.

The ant distribution μ is just the convex combination of the pheromone distribution g and of the isotropic distribution. Therefore, the ant distribution is always smoother than the pheromone distribution. The random velocity jump process, even if very weak, seems to prevent a positive feedback between the ant and pheromone distributions which could lead to the formation of trails. Of course, these conclusions hold only when $\varepsilon \to 0$, i.e. if the equilibrium of the ant jump operator is instantaneously reached. The fact that the simulations do indeed show the formation of trails without any implementation of a preferential choice seems to indicate that the fast microscopic dynamics plays an important role in the formation of trails which the macroscopic model is unable to capture. We also note that if $\sigma = 0$, the pheromone distribution is constant in time. This is due to the fact that, in the absence of random velocity jumps, newly created pheromone particles are deposited according to a distribution which coincides exactly with the current pheromone distribution, resulting in an exact zero balance for this distribution. Therefore, even if $\sigma = 0$, no trails can develop.

Case $k > 1$: existence of a preferential choice. In this case, Eq. (4.31) is a non-local equation due to the operator $g \to g^{[k]}$. No analysis is available yet (to

our knowledge) for such an equation (some preliminary results can be found in [6]). The large-time behavior of the system depends on the limit as $t \to \infty$ of eq. (4.31). We note that (4.31) may produce concentrations [6]. Indeed, the contribution of the largest trails is amplified and the ant flux becomes more strongly correlated to the direction of the largest trails. Therefore if the ants choose preferably the largest trail, the resulting concentration dynamics may counterbalance the effect of the random velocity jumps and a positive feedback between the ants and the pheromone particles is more likely to occur. The study of this case is deferred to future work.

Conclusion on macroscopic models. In the literature, macroscopic models for ant-trail formation are scarce, especially in two spatial dimensions. The models of [17,47] are fluid models (they consider the mean densities of ants and trails), but they are respectively zero and one-dimensional models. Zero-dimensional models merely ignore the spatial dependence and only consider the time evolution of a global particle budget. One-dimensional models are of course unable to give access to the intrinsically two-dimensional topology and geometry of the trail network. In this work, we have derived two-dimensional macroscopic models of ant-trail formation. We have shown that macroscopic models are unable to develop trail formation without some amplification mechanism corresponding to ants choosing the stronger trails with higher probability than the weaker ones. However, at the microscopic level, the need for such an amplification mechanism is not observed (see section 3). This different behavior suggests that macroscopic models may not be valid. Rauch et al [40] argue that the continuous limit of the stochastic particle system must be disregarded. Indeed, simulations at the microscopic level keep track of the internal fluctuations of the system which are believed to be crucial for the emergence of ant-trails. These fluctuations are lost in the continuous limit. We may observe a similar phenomenon here. In the statistical mechanics picture, this may indicate that the chaos property, which is at the foundation of macroscopic models (see e.g. [12]), breaks down. Further rigorous mathematical studies are needed to make this point clearer.

5 Conclusion

In this article, we have introduced an Individual-Based Model of ant-trail formation. The ants are modeled as self-propelled particles which deposit directed pheromone particles (or pieces of trails) and interact with them through alignment interaction. We have introduced a trail detection technique which provides numerical evidence for the formation of trail patterns, and allowed us to quantify the effects of the biological parameters on the pattern formation. Finally, we have proposed both kinetic and fluid descriptions of this model and analyzed the capabilities of the

fluid model to develop trail patterns. This analysis has shown that the concept of a directed pheromone mediated alignment interaction can be a powerful paradigm to understand the emergence and morphologic diversity of ant trails. The propensity to align with neighbors has been recognized as a major component of animal behavior and has been the subject of a vast literature. The present work proposes a new process by which alignment interaction can proceed: instead of being instantaneous in time like in the majority of other works, the interaction is time-delayed through directed pheromone mediation. This results in the emergence of novel morphogenetic features at the level of the population. From the biological viewpoint, the model can be further improved. The ant and pheromone dynamics can be complexified for instance by adding extra pheromone diffusion, anisotropy or saturation in the pheromone detection mechanism, or by investigating the effect of a non-homogeneous medium. From the mathematical viewpoint, a rigorous derivation of the kinetic and fluid equations are still open problems.

Appendix A Trails emerge from pheromone diffusion

The concept of directed pheromone particles introduced in this work is based on the observation that ants lay down regularly spaced pheromone droplets. These droplets are then rapidly connected one to each other by diffusion, forming trails [25]. When they meet such a trail, the ants follow it through an osmotropotaxic response (see section 2.2). In this work, we summarize this process by assuming that the ants deposit signals containing a directional information and modeled by directed pheromone particles. Trail following behavior is modeled by assuming that the ants have some probability of turning towards the direction of one these directed particles when they meet them (i.e. when the detect them within a certain distance).

In this appendix, we simulate the formation of a pheromone trail as a consequence of the deposition of successive droplets and of diffusion. The simulated ant drops 5 pheromones within a short time interval, at intervals of 0.2 s (i.e. at $t = 0, 0.2, 0.4, 0.6, 0.8$ s). Each pheromone droplet has an initial concentration given by a Dirac delta and then spreads away due to diffusion. We use the formula at the bottom of page 301 of [25]. In the simulation, the pheromone diffusion coefficient is $D = 10^{-2}\,\mathrm{cm}^2\,\mathrm{s}^{-1}$ [7] and the ant speed is $c = 2\,\mathrm{cm}\,\mathrm{s}^{-1}$. Thus, the dimensionless parameter $\delta = cd/D$ (where $d = 0.4\,\mathrm{cm}$ is the distance between two pheromones, see section 2.2 for the definition of δ) takes the value $\delta = 80$. Since $\delta \gg 1$, the discrete nature of the deposition process should be observed, at least for a short time. In Fig. 12, we plot the pheromone density (in green) and the ant

position (in blue) in the xy-plane at 4 different times. After 0.5 s, we can clearly distinguish the positions of the 3 pheromone droplets already dropped by the ant. But after 1 s, the ant has dropped 5 pheromone droplets and the pheromone concentration starts to look like a continuous streak. At time $t = 3$ s, the discontinuities due to the discrete deposition process can nonlonger be distinguished and we observe a continuous pheromone trail. After a longer time, the trail disappears due to diffusion. In our model, we only retain the third and fourth stages of this process, and we assume that ants mark small pheromone trails which disappear after some time.

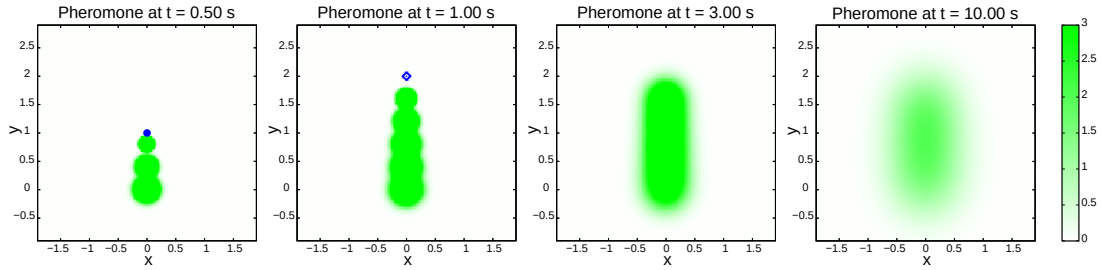


Figure 12: Deposition of successive pheromone droplets that diffuse away. Pheromone concentration (green) and depositing ant position (blue) at $t = 0.5, 3, 5, 10$ s. The droplets are deposited at times $t = 0, 0.2, 0.4, 0.6, 0.8$ s with a concentration given by a Dirac delta. Then the droplet spreads away by diffusion. After time $t = 3$ s, we observe a continuous trail of pheromones. This trail starts to disappear after 10 s. The ant leaves the frame between $t = 1$ s and $t = 3$ s.

References

[1] I. Aoki. A simulation study on the schooling mechanism in fish. Bulletin of the Japan Society of Scientific Fisheries, 48, 1081–1088, 1982.

[2] R. Beckers, J. L. Deneubourg, and S. Goss. Trail laying behaviour during food recruitment in the ant *Lasius niger (L.)*. Insectes Sociaux, 39, 59–72, 1992.

[3] R. Beckers, J. L Deneubourg, S. Goss, and J. M Pasteels. Collective decision making through food recruitment. Insectes Sociaux, 37, 258–267, 1990.

[4] A. Bernadou and V. Fourcassié. Does substrate coarseness matter for foraging ants? an experiment with *Lasius niger (Hymenoptera; formicidae)*. J. Insect Physiol., 54, 534–542, 2008.

[5] A. Blanchet, J. Dolbeault, and B. Perthame. Two-dimensional Keller-Segel model: optimal critical mass and qualitative properties of the solutions. Electron. J. Differential Equations, 44, 1–33, 2006.

[6] E. Boissard and P. Degond. In preparation.

[7] W. H. Bossert, E. O. Wilson. The analysis of olfactory communication among animals J. Theor. Biol., 5, 443–469, 1963.

[8] V. Calenbuhr and J. L Deneubourg. A model for osmotropotactic orientation (I)*. J. Theor. Biol., 158, 359–393, 1992.

[9] V. Calenbuhr, L. Chretien, J. L Deneubourg, and C. Detrain. A model for osmotropotactic orientation (II)*. J. Theor. Biol., 158, 395–407, 1992.

[10] V. Calvez and J. A Carrillo. Volume effects in the Keller-Segel model: energy estimates preventing blow-up. Journal de Mathématiques Pures et Appliquées, 86, 155–175, 2006.

[11] E. Casellas, J. Gautrais, R. Fournier, S. Blanco, M. Combe, V. Fourcassié, G. Theraulaz, and C. Jost. From individual to collective displacements in heterogeneous environments. J. Theor. Biol., 250, 424–434, 2008.

[12] C. Cercignani, R. Illner, and M. Pulvirenti. The mathematical theory of dilute gases. Springer, 1994.

[13] H. Chaté, F. Ginelli, R. Montagne. Simple Model for Active Nematics: Quasi-Long-Range Order and Giant Fluctuations. Phys. Rev. Lett., 96, 180602, 2006.

[14] I. D Couzin and N. R Franks. Self-organized lane formation and optimized traffic flow in army ants. Proceedings of the Royal Society B: Biological Sciences, 270, 139–146, 2003.

[15] J. L Deneubourg, S. Aron, S. Goss, and J. M Pasteels. The self-organizing exploratory pattern of the argentine ant. Journal of Insect Behavior, 3, 159–168, 1990.

[16] C. Detrain, C. Natan, and J. L Deneubourg. The influence of the physical environment on the self-organized foraging patterns of ants. Naturwissenschaften, 88, 171–174, 2001.

[17] L. Edelstein-Keshet. Simple models for trail-following behaviour; trunk trails versus individual foragers. J. Math. Biol., 32, 303–328, 1994.

[18] L. Edelstein-Keshet, J. Watmough, and G. B. Ermentrout. Trail following in ants: individual properties determine population behaviour. Behav. Ecol. Sociobiol., 36, 119–133, 1995.

[19] R. Erban and H. G Othmer. From individual to collective behavior in bacterial chemotaxis. SIAM J. Appl. Math., 70, 361–391, 2004.

[20] G. B Ermentrout and L. Edelstein-Keshet. Cellular automata approaches to biological modeling. J. Theor. Biol., 160, 97–133, 1993.

[21] F. Filbet, P. Laurençot, and B. Perthame. Derivation of hyperbolic models for chemosensitive movement. J. Math. Biol., 50, 189–207, 2005.

[22] S. Goss, S. Aron, J. L Deneubourg, and J. M Pasteels. Self-organized shortcuts in the argentine ant. Naturwissenschaften, 76, 579–581, 1989.

[23] P. P Grassé. Termitologia: comportement, socialité, écologie, évolution, systématique. Masson, 1986.

[24] D. Grünbaum. Align in the sand. Science, 312, 1320-1322, 2006.

[25] J. W. Haefner, T. O. Crist. Spatial model of movement and foraging in harvester ants *(Pogonomyrmes)* (I): the roles of memory and communication. J. Theor. Biol., 166, 299–313, 1994.

[26] W. Hangartner. Trail laying in the subterranean ant, *Acanthomyops interjectus*. J. Insec. Physiol., 15, 1–4, 1969.

[27] T. Hillen and H. G Othmer. The diffusion limit of transport equations derived from velocity-jump processes. SIAM J. Appl. Math., 61, 751–775, 2000.

[28] D. E. Jackson, N. Châline. Modulation of pheromone trail strength with food quality in Pharaoh's ant, *Monomorium pharaonis*. Animal Behaviour, 74, 463–470, 2007.

[29] R. Jeanson, J-L. Deneubourg, A. Grimal, G. Theraulaz. Modulation of individual behavior and collective decision-making during aggregation site selection by the ant *Messior barbarus*. Behav. Ecol. Sociobiol., 55, 388–394, 2004.

[30] A. John, A. Schadschneider, D. Chowdhury, and K. Nishinari. Collective effects in traffic on bi-directional ant trails. J. Theor. Biol., 231, 279–285, 2004.

[31] Y. Katz, K. Tunstrom, C. C. Ioannou, C. Huepe, I. D. Couzin, Inferring the structure and dynamics of interactions in schooling fish. Proc. Nat. Acad. Sci., 108, 18720-18725, 2011.

[32] E. F Keller and L. A Segel. Model for chemotaxis. J. Theor. Biol., 30, 225–234, 1971.

[33] R. Lukeman, Y-X. Li, L. Edelstein-Keshet. Inferring individual rules from collective behavior Proc. Nat. Acad. Sci. 107, 12576-12580, 2010.

[34] E. D. Morgan. Trail pheromones of ants Physiological Entomology, 34, 1–17, 2009.

[35] K. Nishinari, K. Sugawara, T. Kazama, A. Schadschneider, and D. Chowdhury. Modelling of self-driven particles: Foraging ants and pedestrians. Physica A: Statistical Mechanics and its Applications, 372, 132–141, 2006.

[36] H. G Othmer and T. Hillen. The diffusion limit of transport equations II: chemotaxis equations. SIAM J. Appl. Math., 62, 1222–1250, 2002.

[37] H. G Othmer and A. Stevens. Aggregation, blowup, and collapse: The ABC's of taxis in reinforced random walks. SIAM J. Appl. Math., 57, 1044–1081, 1997.

[38] K. J. Painter. Modelling cell migration strategies in the extracellular matrix. J. Math. Biol., 58, 511–543, 2009.

[39] K. Peters, A. Johansson, A. Dussutour, and D. Helbing. Analytical and numerical investigation of ant behavior under crowded conditions. Advances in Complex Systems, 9, 337–352, 2006.

[40] E. M. Rauch, M. M. Millonas, and D. R. Chialvo. Pattern formation and functionality in swarm models. Physics Letters A, 207, 185–193, 1995.

[41] F. Schweitzer, K. Lao, and F. Family. Active random walkers simulate trunk trail formation by ants. BioSystems, 41, 153–166, 1997.

[42] A. Stevens. The derivation of chemotaxis equations as limit dynamics of moderately interacting stochastic many-particle systems. SIAM J. Appl. Math., 61, 183–212, 2000.

[43] O. G. Sutton. Micrometeorology. McGraw Hill, New-York, 1953.

[44] T. Tao, H. Nakagawa, M. Yamasaki, and H. Nishimori. Flexible foraging of ants under unsteadily varying environment. Journal of the Physical Society of Japan, 73, 2333–2341, 2004.

[45] T. Vicsek, A. Czirók, E. Ben-Jacob, I. Cohen, O. Shochet, Novel type of phase transition in a system of self-driven particles. Phys. Rev. Lett., 75, 1226–1229, 1995.

[46] A. D Vincent and M. R Myerscough. The effect of a non-uniform turning kernel on ant trail morphology. J. Math. Biol., 49, 391–432, 2004.

[47] J. Watmough and L. Edelstein-Keshet. A one dimensional model of trail propagation by army ants. J. Math. Biol., 33, 459–476, 1995.

[48] J. Watmough and L. Edelstein-Keshet. Modelling the formation of trail networks by foraging ants. J. Theor. Biol., 176, 357–371, 1995.

[49] E. O. Wilson. Chemical communication among workers of the fire ant *Solenopsis saevissima (Fr. Smith)* 1. the organization of mass-foraging. Animal Behaviour, 10, 134:147, 1962.

[50] V. Witte, U. Maschwitz. Coordination of raiding and emigration in the ponerine army ant *Leptogenys distinguenda (Hymenoptera: Formicidae: Ponerinae)* J. Insect Behav., 15, 195–217, 2002.